Key trends in the response of suction bucket foundations to extreme axial cyclic loads

Grecu, Sorin; Barari, Amin; Ibsen, Lars Bo

Published in:
Soil Dynamics and Earthquake Engineering

DOI (link to publication from Publisher):
10.1016/j.soildyn.2023.108344

Publication date:
2024

Document Version
Publisher's PDF, also known as Version of record

Citation for published version (APA):
Grecu, S., Barari, A., & Ibsen, L. B. (2024). Key trends in the response of suction bucket foundations to extreme axial cyclic loads. *Soil Dynamics and Earthquake Engineering*, *176*, Article 108344. https://doi.org/10.1016/j.soildyn.2023.108344

Soil Dynamics and Earthquake Engineering 176 (2024) 108344

Contents lists available at ScienceDirect

Soil Dynamics and Earthquake Engineering

journal homepage: www.elsevier.com/locate/soildyn

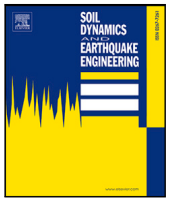

Key trends in the response of suction bucket foundations to extreme axial cyclic loads

Sorin Grecu [a,*], Amin Barari [a,b], Lars Bo Ibsen [a]

[a] Department of the Built Environment, Aalborg University, Thomas Manns Vej 23, Aalborg East, 9220, Denmark
[b] School of Engineering, RMIT University, Melbourne, VIC 3000, Australia

ARTICLE INFO

Keywords:
Bucket foundation
Cyclic loading
Stiffness degradation
Liquefaction
Physical modeling

ABSTRACT

The offshore wind industry is currently expanding into emerging markets at a rapid pace. Some of these markets are located in areas characterized by frequent extreme events. From a geotechnical perspective, this results in new design challenges, as foundations must withstand severe loads repeatedly throughout their intended lifetimes. Jacket structures resting on suction buckets represent a new foundation concept that still requires research to become a potential optimal solution. The vertical cyclic response of bucket foundations constitutes the main topic of this article. The current study is based on observations of the behavior of a scaled model installed in dense sand. Both normal and extreme conditions were simulated by applying axial cyclic loads of varying amplitudes, means, and frequencies. High amplitude and low frequency cause significant stiffness degradation and permanent displacement. These scenarios occur due to build-up of excess pore pressure, with subsequent triggering of liquefaction. A criterion for liquefaction occurrence is identified and may be readily used for practical applications. Considerable levels of tensile loading lead to a high rate of heave, regardless of frequency. For one-way compressive forces, after an extreme loading sequence, stiffness returns to its initial level, as long as no liquefaction develops priorly. This bears essential implications in predicting the change of natural frequency of the system.

1. Introduction

The offshore wind industry has been expanding rapidly in recent years and continues to do so at the time of writing. As its progress relies partly on evolution of offshore wind turbine (OWT) technology, there exists motivation and need for research on novel concepts pertaining to various turbine components. One critically important area of development comprises support structures and foundations, as these must ensure stability and serviceability throughout the intended lifetime. With turbines becoming larger and farms being constructed in deeper waters, new foundation solutions are actively sought.

A viable candidate comes in the form of steel latticework supported by suction buckets (or caissons), commonly referred to as "suction bucket jacket" (SBJ). Some circumstances may favor SBJs instead of monopiles, particularly when heavier turbines and water depths larger than 30 m are involved. As a concept, the SBJ system has existed since the 1990s, with instances of full-scale validation taking place at several locations in the North Sea over the years [1]. Recently, this foundation solution has been applied to all turbines within Aberdeen Bay and Seagreen offshore wind farms. While Northwest Europe leads offshore wind globally, North America and Asia Pacific represent large emerging markets [2]. From a foundation design standpoint, a key issue is that local European expertise cannot be readily and directly exported to the aforementioned areas. This is due to new environmental challenges, such as relatively frequent earthquakes and tropical cyclones, which may be of critical importance for designing OWTs installed near the shores of some countries, such as Taiwan, Japan, South Korea, China, and the USA. Therefore, many uncertainties related to SBJ performance stem from the novelty of both technology and natural surroundings.

In a marine environment, such structures are constantly subjected to cyclic loads caused by wind turbulence and waves. Earthquakes or extreme sea conditions can trigger seabed liquefaction, which marks a vulnerability of SBJs in highly disaster-prone regions [3–6]. Moreover, in the special case of OWTs, rotor imbalances and blade shadowing impose additional forces, known as 1P and 3P loads, respectively [7]. The primary components of all mentioned forces are horizontal, and lead to overturning moments that translate to vertical loading at the foundation level [8,9]. This load-transfer mechanism, inherent to multi-footed substructures and generally called "push–pull", is depicted in Fig. 1. It becomes evident that individual footings always experience vertical cyclic loading.

* Corresponding author.
E-mail address: sgre@build.aau.dk (S. Grecu).

https://doi.org/10.1016/j.soildyn.2023.108344
Received 11 April 2023; Received in revised form 4 October 2023; Accepted 3 November 2023
Available online 10 November 2023

Nomenclature

A_o	outer lid area
A_{loop}	hysteresis loop area
CPT	cone penetration test
D_i	inner lid diameter
D_o	outer lid diameter
D_r	relative density
d_{50}	median grain diameter
EPWP	excess pore water pressure
e_{max}	maximum void ratio
e_{min}	minimum void ratio
F_0	force at pre-shearing phase start
F_{cyc}	force amplitude
F_{max}	maximum force within a cycle
F_{mean}	mean force within a cycle
F_{min}	minimum force within a cycle
F_{press}	force due to pressurization
F_{proc}	processed force readings
F_{raw}	raw force readings
F_z	vertical force
f	loading frequency
G_S	specific gravity
K_{un}	unloading stiffness
$K_{un,end}$	K_{un} at the last cycle
$K_{un,initial}$	K_{un} at the first cycle
L_i	inner skirt length
L_o	outer skirt length
LVDT	linear variable differential transformer
m	mass
N	number of cycles
OWT	offshore wind turbine
q_c	cone resistance
R_t^d	drained tensile capacity
SBJ	suction bucket jacket
$d_{60/10}$	uniformity coefficient
t_{lid}	lid plate thickness
t_{skirt}	skirt plate thickness
ULS	ultimate limit state
u_e	excess pore pressure
$u_{e,max}$	maximum u_e within a cycle
$u_{e,mean}$	mean u_e within a cycle
$u_{e,min}$	minimum u_e within a cycle
W'_m	effective weight of the model
z	vertical displacement
z_{loop}	range of z within a cycle
z_{max}	maximum z within a cycle
z_{mean}	mean z within a cycle
z_{min}	minimum z within a cycle
$(z/D_o)_p$	normalized z at the end of a load packet
$(z/D_o)_t$	normalized z at the end of a test
γ'	effective unit weight
σ'_v	effective vertical stress
ψ	dilation angle
*	normalized quantity

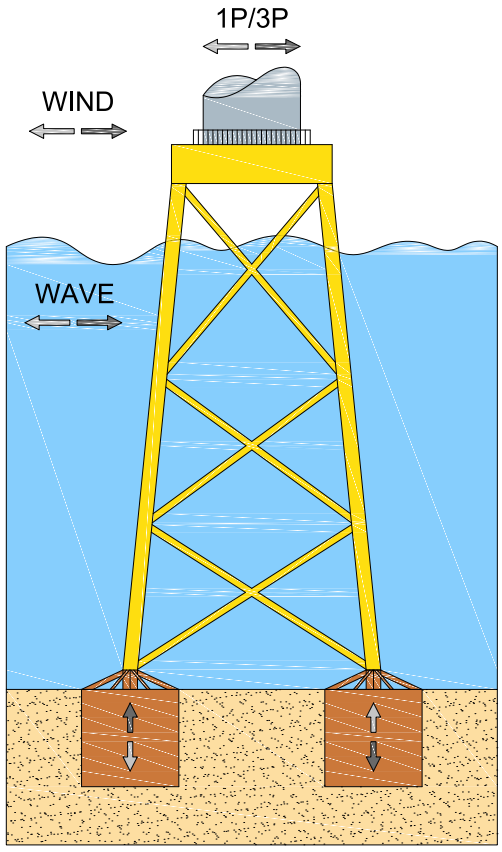

Fig. 1. The load-transfer mechanism characteristic to jacket structures.

Table 1
Model properties.

Parameter name (symbol)	Value	Unit
Outer diameter (D_o)	500	mm
Inner diameter (D_i)	492	mm
Outer skirt length (L_o)	510	mm
Inner skirt length (L_i)	498	mm
Lid plate thickness (t_{lid})	12	mm
Skirt plate thickness (t_{skirt})	4	mm
Mass (m)	65.24	kg

Table 2
Properties of Baskarp Sand no. 15.

Parameter name (symbol)	Value	Unit
Maximum void ratio (e_{max})	0.854	–
Minimum void ratio (e_{min})	0.549	–
Median grain diameter (d_{50})	0.14	mm
Uniformity coefficient (d_{60}/d_{10})	1.78	–
Specific gravity (G_S)	2.64	–

The cyclic response of suction buckets represents an active topic of research, since there is insufficient knowledge and experience that could form the basis for a design framework. Observations from full-scale examples, which constitute the most valuable resource, are rather scarce and not publicly available. Instead, numerical and experimental studies generate most of the accessible knowledge. This paper falls into the latter category, as it describes the output of a laboratory testing campaign.

Foundation behavior exhibits dependency on all cyclic loading characteristics: amplitude, mean load, frequency, direction, and number of cycles. Trends in soil–structure interaction may be affected temporarily, as well as permanently. This can be deduced from Shonberg et al. [10], who present in-situ observations of an instrumented SBJ at prototype

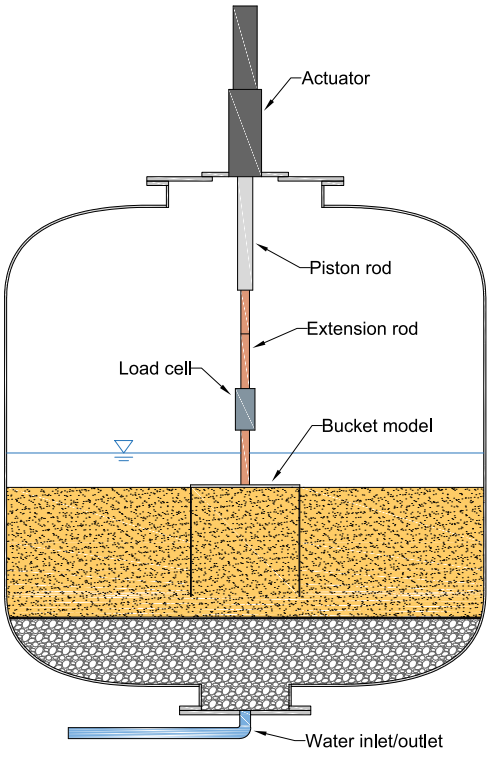

Fig. 2. Cross-section containing the system's axis of symmetry.

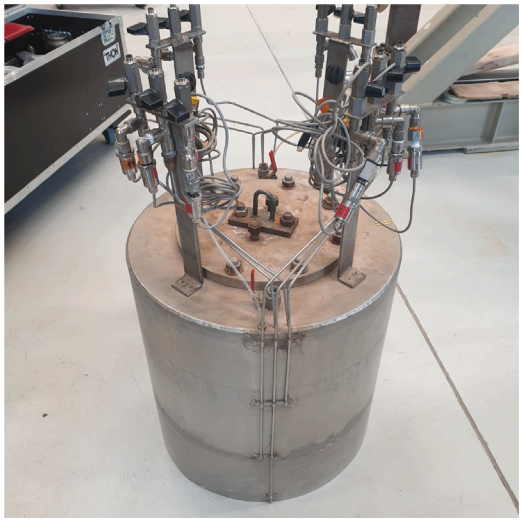

Fig. 3. The suction bucket model.

scale. Further evidence is found in the experimental works of Byrne and Houlsby [11], Kelly et al. [12,13], Chen and Randolph [14], Hung et al. [15], Nielsen et al. [16], Vaitkune et al. [17], Bienen et al. [18], Gütz [19], Jeong et al. [20,21,22], Low et al. [23], Stapelfeldt et al. [24,25], Zhang et al. [26], Zhao et al. [27], Gütz and Achmus [28], Grecu et al. [29].

Most of the cited research commonly concludes that cyclic loading in pure compression is not likely to raise concerns regarding ULS design cases. This loading regime corresponds to a normal sea state and accounts for the major part of an OWT's lifetime. Under such conditions, depending on the operation status and weight of the structure, the vertical compressive force on windward legs might reduce in magnitude without a change of sign [18]. On the other hand, pure tensile and

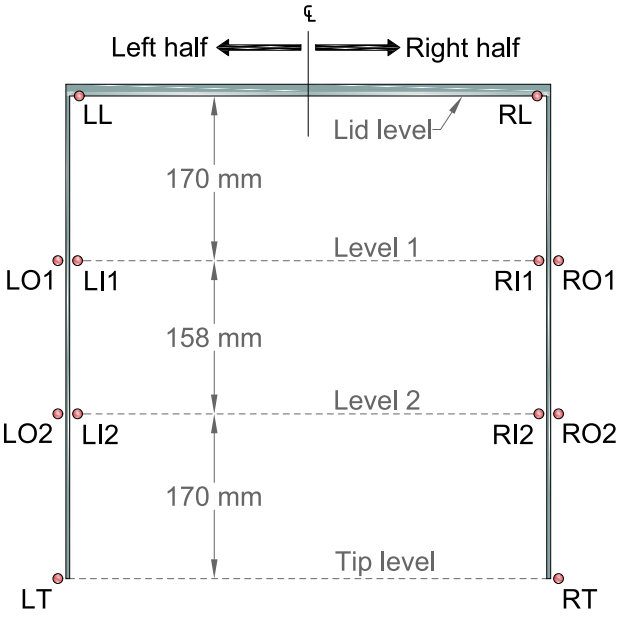

Fig. 4. Cross-section containing the model's axis of symmetry. The red dots indicate the locations of pressure reading points.

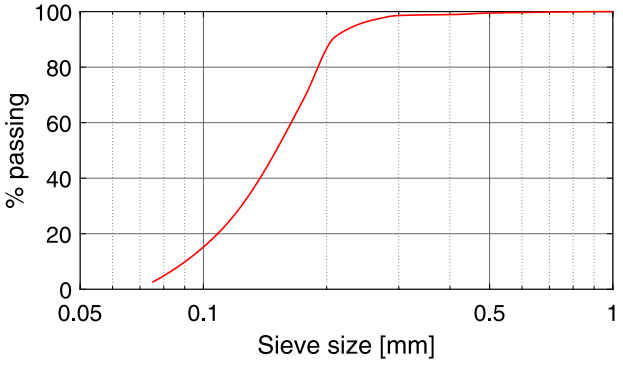

Fig. 5. Grain size distribution curve of Baskarp Sand no. 15.

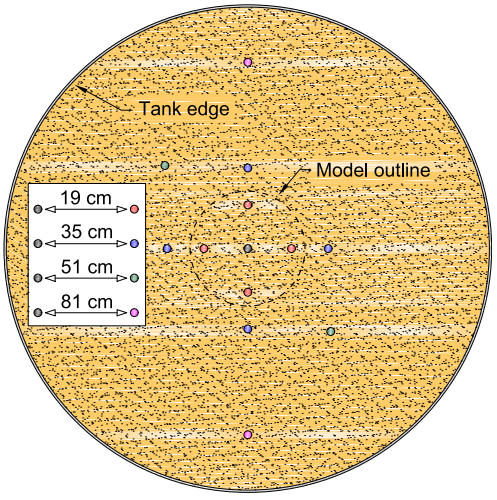

Fig. 6. CPT locations. The black dot marks the geometric center of the model and tank.

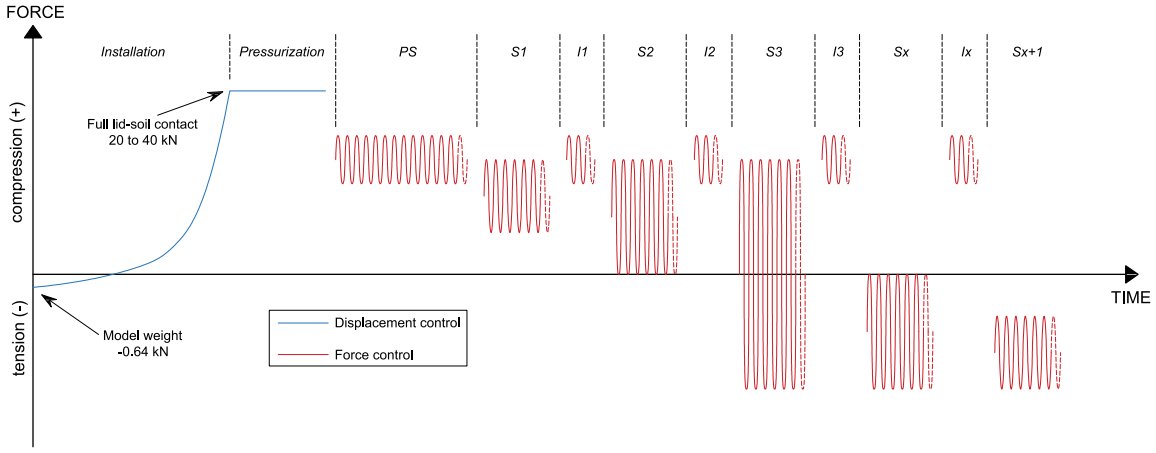

Fig. 7. Schematic of test phases; where *PS* – pre-shearing packet, *S* – severe load packet, and *I* – intermediate packet.

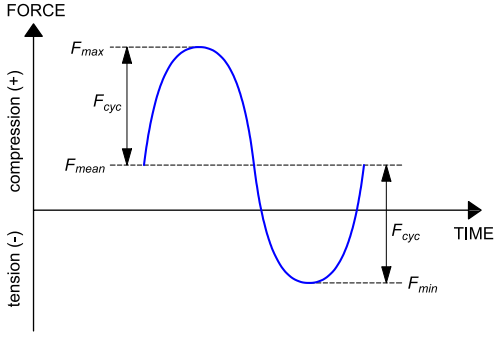

Fig. 8. Definitions of cyclic load parameters.

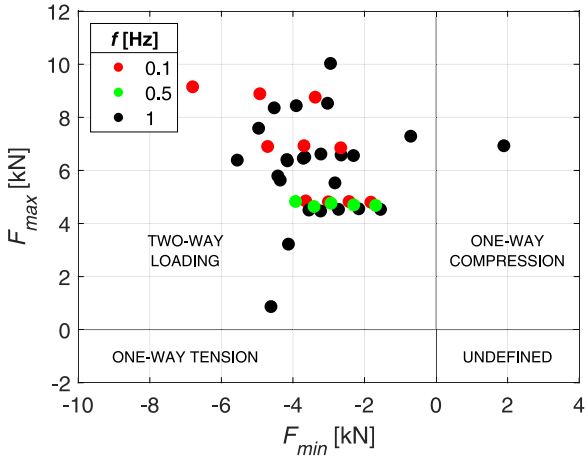

Fig. 9. Characteristics of S-packets.

Table 3
Normalized quantities.

Parameter name (symbol)	Group
Vertical displacement (z)	$z^* = z/D_o$
Vertical force (F_z)	$F_z^* = F_z/(\gamma' D_o^3)$
Unloading stiffness (K_{un})	$K_{un}^* = K_{un}/(\gamma' D_o^2)$

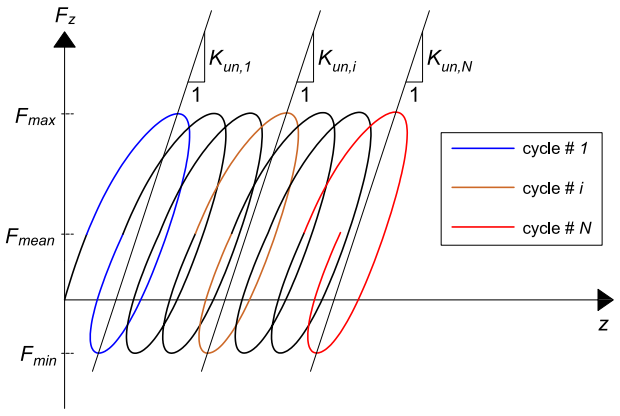

Fig. 10. Definition of unloading stiffness.

two-way cyclic loading are considerably more onerous scenarios for bucket foundations. They typically occur during severe and relatively short events, such as storms. These loading conditions require thorough consideration in the design process, since they may cause irreparable damage.

Lack of engineering practice with SBJs in liquefiable seabed leads to large risks for all stakeholders, and potentially increases project costs. The offshore wind industry is expanding towards regions prone to frequent natural disasters, which adds to the relevance of investigating OWT foundations subjected to severe loads. Although several design guidelines have already been developed [30,31], there is still limited field and laboratory data that could form a basis for thorough understanding of the consequences of significant environmental forces on foundation response. This often results in conservatism as a measure to account for uncertainties, which affects project economy, given the substantial cost share of foundations [7].

This research places its main focus on critical loading scenarios. A set of tests are conducted using a model of a suction bucket installed in dense sand in a pressurized environment. Vertical force is imposed onto the model via a hydraulic actuator, in manners dictated by target force time series. The essential idea is to systematically vary the parameters of the applied regular load waveforms and examine the model response. The study involves three independent variables: amplitude, mean load, and frequency. Model geometry and soil properties are held constant across tests, in order to isolate the effects of cyclic load characteristics.

The main goal is to gain insight into the vertical cyclic behavior of suction buckets as parts of SBJs during extreme events. Specifically,

Table 4
The testing program (tests 1–6).

Test #	D_r [%]	γ' [kN/m^3]	Packet #	Packet ID	N #	F_{mean} [kN]	F_{cyc} [kN]	F_{max} [kN]	F_{min} [kN]	f [Hz]	$(z/D_o)_t$ $\times 10^{-3}$ [–]	$(z/D_o)_p$ $\times 10^{-3}$ [–]
1	85.3	10.10	1	PS	1000	5.6	2.1	7.6	3.5	0.1	0.4	0.4
			2	S1	434	−0.5	3.7	3.2	−4.1	1	−219.71	−220.11
2	84.9	10.1	1	PS	1000	5.6	2.1	7.6	3.5	0.1	0.45	0.45
			2	S1	162	−1.9	2.7	0.9	−4.6	1	−235.59	−236.05
3	85	10.1	1	PS	1000	5.6	2	7.6	3.5	0.1	0.39	0.39
			2	S1	499	2.1	4.4	6.6	−2.3	1	2.52	2.14
			3	I1	200	5.6	2	7.6	3.5	0.1	3.37	0.85
			4	S2	499	1.7	4.9	6.6	−3.2	1	6.06	2.69
			5	I2	200	5.6	2	7.6	3.5	0.1	7.04	0.98
			6	S3	499	1.4	5.1	6.5	−3.7	1	7.18	0.14
			7	I3	200	5.6	2.1	7.6	3.5	0.1	9.52	2.34
			8	S4	499	1.1	5.3	6.4	−4.2	1	4.62	−4.9
			9	I4	200	5.6	2.1	7.6	3.5	0.1	9.96	5.34
			10	S5	499	0.7	5.1	5.8	−4.4	1	−61.08	−71.04
4	84.3	10	1	PS	1000	5.6	2	7.6	3.5	0.1	0.33	0.33
			2	S1	498	1.4	5.1	6.5	−3.7	1	−4.2	−4.53
			3	I1	200	5.6	2	7.6	3.5	0.1	−1.87	2.33
			4	S2	498	1.1	5.3	6.4	−4.2	1	−17.06	−15.19
			5	I2	200	5.6	2	7.6	3.5	0.1	−12.31	4.75
			6	S3	498	0.6	5	5.6	−4.4	1	−94.3	−81.99
5	86.1	10.1	1	PS	1000	5.6	2.1	7.6	3.5	0.1	0.09	0.09
			2	S1	500	2.1	4.8	6.9	−2.7	0.1	0.94	0.85
			3	I1	200	5.6	2.1	7.6	3.5	0.1	1.72	0.78
			4	S2	500	1.6	5.3	6.9	−3.7	0.1	−139.33	−141.05
			5	I2	200	5.6	2	7.6	3.5	0.1	−130.68	8.65
			6	S3	88	1.1	5.8	6.9	−4.7	0.1	−258.83	−128.15
6	85.5	10	1	PS	1000	5.6	2.1	7.6	3.5	0.1	0.33	0.33
			2	S1	500	1.5	3.3	4.8	−1.8	0.1	0.06	−0.26
			3	I1	200	5.6	2	7.6	3.5	0.1	1.08	1.02
			4	S2	500	1.2	3.6	4.8	−2.4	0.1	0.69	−0.39
			5	I2	200	5.6	2.1	7.6	3.5	0.1	1.93	1.24
			6	S3	500	0.9	3.9	4.8	−3	0.1	−30.94	−32.87
			7	I3	200	5.6	2.1	7.6	3.5	0.1	−25.48	5.46
			8	S4	149	0.6	4.2	4.9	−3.6	0.1	−239.05	−213.57

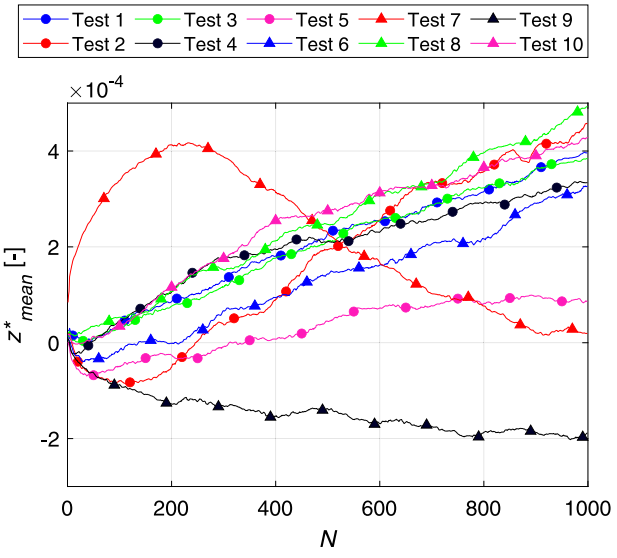

Fig. 11. Normalized mean vertical displacements from PS-packets.

accumulated displacements and stiffness are emphasized, since these variables appear of most interest for practical applications. To achieve the set aims, in each test, loading starts as a series of one-way compression cycles, and progresses towards pure tension in a stepwise pattern. This unique approach of modeling the load regime transition allows describing the evolution of the foundation response with increasing severity level of an event.

Several observed trends emerge as the key findings of the current study:

- A high cyclic loading amplitude at low frequency appears as the most damaging loading scenario, causing significant stiffness degradation and permanent settlement.
- Plug heave can occur under significant load levels. This phenomenon is further enhanced at lower frequencies.
- The soil–foundation system regains its initial stiffness when subjected to one-way compressive forces after an extreme loading scenario, except when preceded by liquefaction.

The obtained insight adds to the existing pool of knowledge on the subject of suction bucket jackets as foundation solution for offshore wind turbines and bears high relevance to the prediction of performance under severe environmental conditions. These findings improve the understanding of risks associated with soil–structure interaction, particularly during liquefaction.

2. Experimental setup and program

2.1. Testing equipment

The experiments were conducted in a sealed tank of cylindrical shape, which has an inner height and diameter of 2.1 m; see the sketch in Fig. 2. Loading was applied using a hydraulic actuator mounted on top of the tank. To compensate for the insufficient stroke length,

Table 5
The testing program (tests 7–10).

Test #	D_r [%]	γ' [kN/m^3]	Packet #	Packet ID	N #	F_{mean} [kN]	F_{cyc} [kN]	F_{max} [kN]	F_{min} [kN]	f [Hz]	$(z/D_o)_t$ $\times 10^{-3}$ [–]	$(z/D_o)_p$ $\times 10^{-3}$ [–]
			1	PS	1000	5.6	2	7.6	3.5	0.1	0.02	0.02
			2	S1	497	1.5	3	4.5	−1.6	1	−0.57	−0.59
			3	I1	200	5.6	2	7.6	3.5	0.1	0.51	1.07
			4	S2	497	1.2	3.4	4.6	−2.2	1	−0.15	−0.66
7	87.1	10.1	5	I2	200	5.6	2	7.6	3.5	0.1	1.06	1.21
			6	S3	497	0.9	3.6	4.5	−2.7	1	0.3	−0.76
			7	I3	200	5.6	2	7.6	3.5	0.1	1.62	1.31
			8	S4	497	0.6	3.8	4.5	−3.2	1	0.04	−1.58
			9	I4	200	5.6	2	7.6	3.5	0.1	1.75	1.7
			10	S5	497	0.5	4	4.5	−3.6	1	−4	−5.75
			1	PS	1000	5.6	2	7.6	3.5	0.1	0.49	0.49
			2	S1	499	1.5	3.2	4.7	−1.7	0.5	−0.08	−0.57
			3	I1	200	5.6	2.1	7.6	3.5	0.1	0.95	1.03
			4	S2	499	1.2	3.5	4.7	−2.3	0.5	0.4	−0.55
8	86.1	10.1	5	I2	200	5.6	2	7.6	3.5	0.1	1.44	1.03
			6	S3	499	0.9	3.8	4.8	−2.9	0.5	0.54	−0.9
			7	I3	200	5.6	2	7.6	3.5	0.1	1.67	1.13
			8	S4	499	0.6	4	4.6	−3.4	0.5	−1.78	−3.45
			9	I4	200	5.6	2	7.6	3.5	0.1	0.19	1.97
			10	S5	499	0.5	4.4	4.8	−3.9	0.5	−38.28	−38.47
			1	PS	1000	5.6	2	7.6	3.5	0.1	−0.19	−0.19
			2	S1	500	2.7	6.1	8.8	−3.4	0.1	2.21	2.4
9	87.5	10.1	3	I1	200	5.6	2	7.6	3.5	0.1	4.01	1.8
			4	S2	500	2	6.9	8.9	−4.9	0.1	−79.1	−83.11
			5	I2	200	5.6	2	7.6	3.5	0.1	−46.9	32.2
			6	S3	26	1.2	8	9.2	−6.8	0.1	−195.31	−148.4
			1	PS	1000	5.6	2	7.6	3.5	0.1	0.43	0.43
			2	S1	496	2.7	5.8	8.5	−3	1	7.98	7.55
			3	I1	200	5.6	2	7.6	3.5	0.1	8.77	0.8
			4	S2	496	2.3	6.2	8.4	−3.9	1	20.35	11.58
10	85.8	10	5	I2	200	5.6	2	7.6	3.5	0.1	22.21	1.86
			6	S3	496	1.9	6.4	8.4	−4.5	1	26.79	4.58
			7	I3	200	5.6	2.1	7.6	3.5	0.1	30.22	3.43
			8	S4	496	1.3	6.3	7.6	−5	1	7.55	−22.66
			9	I4	200	5.6	2	7.6	3.5	0.1	33.13	25.58
			10	S5	496	0.4	6	6.4	−5.6	1	−87.41	−120.54

extension rods were attached to the piston rod. Water was stored in a container placed 7.5 m above the room floor and was supplied through the bottom of the tank. The water surface level was approximately 15 cm above the soil surface level. The soil medium comprised two layers, separated by a permeable membrane: 0.6 m of sand overlaying 0.3 m of gravel.

The suction bucket model used across all tests was made of stainless steel and was instrumented with 12 pressure transducers mounted to the lid via 4 columns, as seen in Fig. 3. The transducers read pore pressure at various points across the skirt surface through steel straws, which were fully saturated before each test. The cross-section of the model and details on pressure reading points are illustrated in Fig. 4. Information regarding model geometry and mass is presented in Table 1.

An LVDT embedded within the actuator measured vertical displacements. Forces were read by a load cell mounted between extension rods. All sensing devices were checked and recalibrated as necessary before each test. A centralized acquisition system recorded data at a sampling frequency of 256 Hz.

2.2. Soil preparation and properties

The testing medium was Baskarp Sand no. 15, which is a fine, uniformly-graded quartz sand. Documentation of its properties is found in Ibsen and Bødker [32]. Fig. 5 shows the particle size distribution, plotted according to data from Borup and Hedegaard [33]. Basic parameters are summarized in Table 2.

The average relative density (D_r) of sand was 85 %, with a standard deviation of 1.9 %. The compaction process before each test consisted of inserting a vibrating rod vertically at multiple locations, covering the entire soil surface. This procedure would be repeated as many times as required to meet a pre-established criterion of minimum average D_r of 80 %. A total of 12 CPTs were performed in connection with each test, at locations indicated in Fig. 6, using a mini-cone with a radius of 7.5 mm and pressed at a rate of 5 mm/s. This piece of equipment, developed at Aalborg University, is smaller than a standard cone; thus, common methods for deriving density based on CPT results could not be employed. Instead, a relationship between cone resistance (q_c) and D_r, formulated specifically for the mini-cone and Baskarp Sand no. 15 [34], was applied.

2.3. Test phases and program

Fig. 7 provides a conceptual depiction of test phases. The same approach is adopted in every test, where cyclic loads progress from one-way compression to one-way tension, but with varying characteristics between tests.

The test stages are described as follows:

- *Installation.* The model is installed by jacking, with no suction assistance. The lid is equipped with two valves, which are kept open during the entire process, in order to avoid insertion of air bubbles in the soil volume and prevent generation of excess pore pressure. Before the skirt tip makes contact with the soil surface, the load cell reads approximately −0.64 kN, which is the weight of the model, including all attachments. Installation ends when full contact between the soil and lid occurs. This is determined by monitoring the load cell readings and visually inspecting the model at the same time. Two indicators of full contact are followed: (1) force starts to increase exponentially;

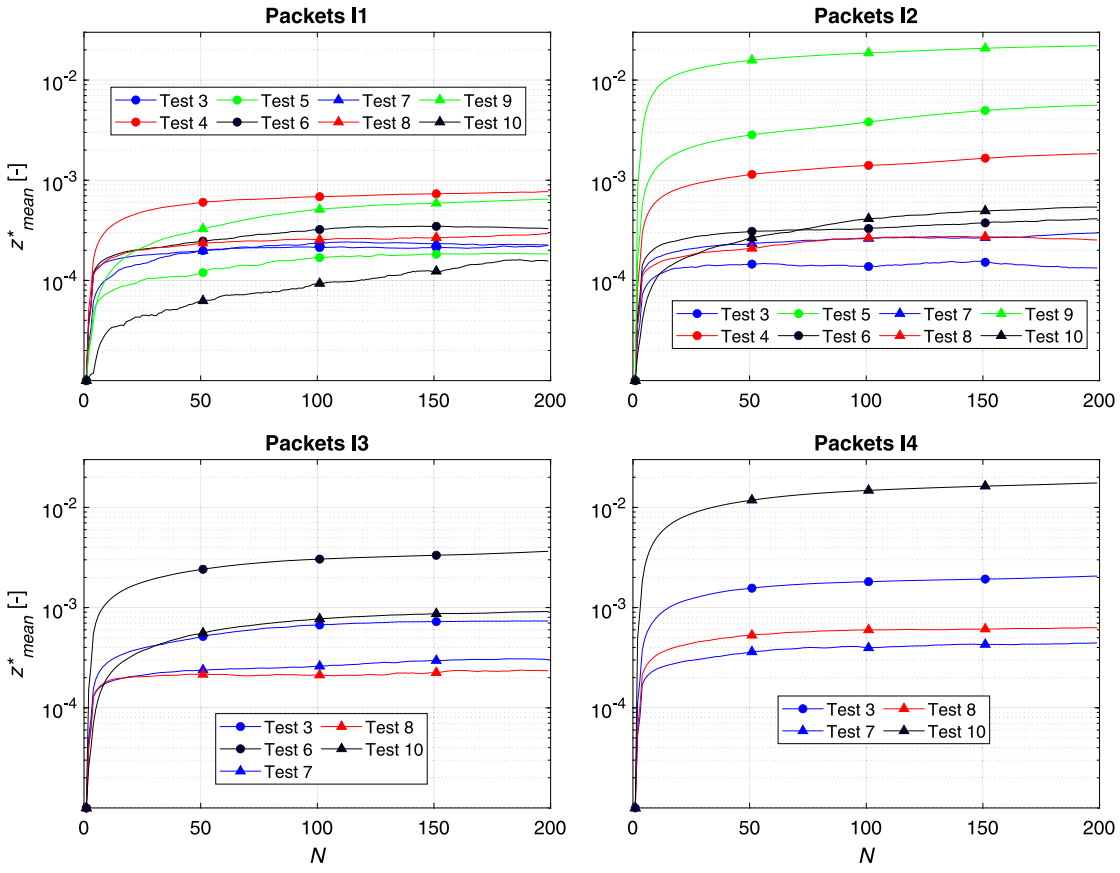

Fig. 12. Normalized mean vertical displacements from I-packets.

(2) water expelled from the space between the lid and soil flows at a slower rate and contains sand grains.

- *Pressurization.* The ambient pressure is increased by 200 kPa, which reflects seabed conditions at 20 m of water depth. Pressurization increases the chances of complete saturation of soil and lowers the cavitation pressure from −100 kPa to −300 kPa, which is especially relevant to suction buckets, since the amount of possible suction pressure defines an upper limit for tensile resistance [13].
- *PS- and I-packets.* All intermediate and pre-shearing packets are characterized by the same mean force (5.6 kN), amplitude (2.1 kN), and frequency (0.1 Hz). These stages are intended to simulate normal operating conditions. The mean force is taken as the sum of 1 % of the vertical bearing capacity, estimated according to Barari et al. [35], and submerged weight of the model. The choice of frequency is governed by the intention to avoid a build-up of excess pore pressure. However, the amplitude values appear as a consequence of technical limitations of the actuator, as it is not possible to achieve smaller values. The *I*-packets contain 200 cycles, while *PS* contains 1000 cycles. The intermediate phases make it possible to observe the effects of preceding severe loading scenarios. *PS* captures the bedding-in process that would take place after the installation and until the first extreme event [36].
- *S-packets.* These loading sequences simulate significant events. They differ in their parameters across tests and represent the main variables in this study.

The parameters describing any force cycle are defined in Fig. 8. The subscripts "max", "min", "cyc", and "mean" apply to other variables as well, e.g., displacement, pore pressure, stress, to describe their cyclic characteristics. The subscript "z" denotes vector quantities that are parallel to the axis of symmetry of the suction bucket.

Throughout this paper, the force readings are presented in their processed form, obtained with Eq. (1).

$$F_{proc} = F_{raw} - F_{press} - W'_m \tag{1}$$

where F_{proc} — processed force readings, F_{raw} — raw force readings, F_{press} — compression effect of pressurization on the load cell (2.32 kN), and W'_m — effective weight of the model (−0.567 kN). A consequence of applying Eq. (1) is that F_{proc} represents a force acting directly on the soil, instead of on the model lid. Vertical displacement, normalized with respect to outer lid diameter (z/D_o), takes positive values for settlement (downward displacement), and negative for heave (upward displacement).

The testing program is outlined in Table 4 and Table 5, where γ' is the effective unit weight, N is the number of applied force cycles, f denotes loading frequency, $(z/D_o)_t$ and $(z/D_o)_p$ refer to accumulated vertical displacements at the end of a phase relative to initial position at the test start and phase start, respectively. In the text, specific packets are referred to by test number and packet identifier. For example, 5-S2 denotes packet S2 in test 5.

Several tests were interrupted due to accumulated displacements reaching predefined safety limits. The lower bound of position was implemented to prevent cables from sinking and the permeable membrane from being cut through by the skirt tip; while the upper bound ensured that equipment would not be damaged upon complete loss of tensile resistance, as the actuator would generate high uplift rates in force-control mode. However, achieving these limits is still relevant to the study, since it implies foundation failure.

Fig. 9 provides a graphical summary of characteristics of S-packets. The main study focus relates to two-way loading, as suggested by the concentration of data points in the upper left quadrant. On the other hand, the absence of tests involving one-way tension is due to either the inability of the model to tolerate such loading, which was also observed

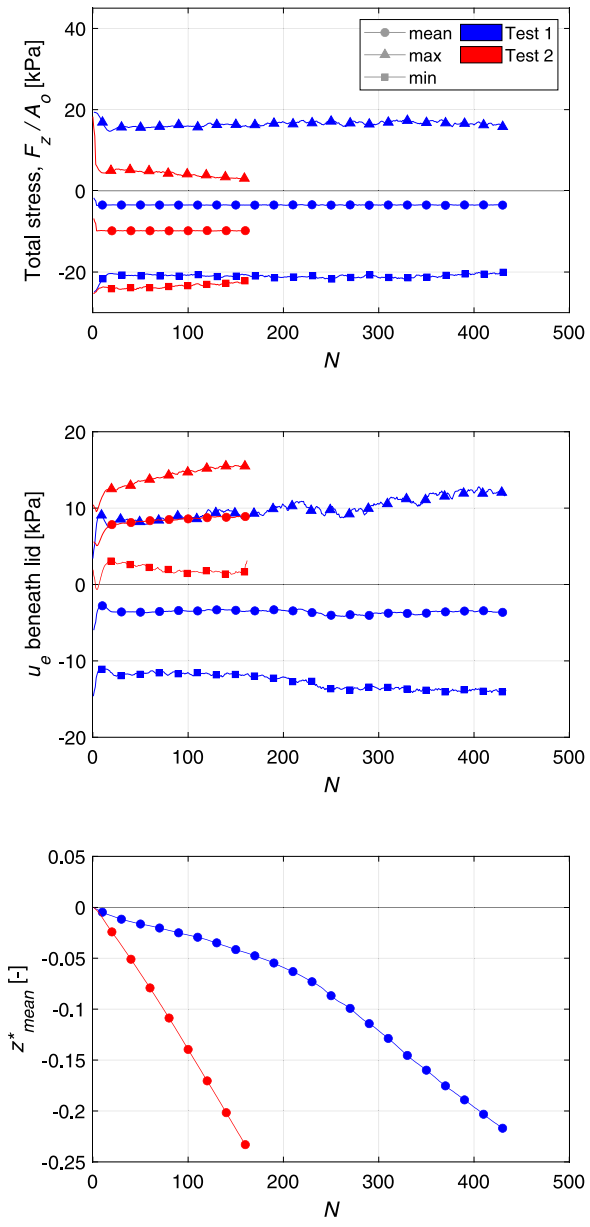

Fig. 13. Output from packets S1. Loading frequency $f = 1$ Hz.

by Bienen et al. [18]; or failure occurring during an earlier loading sequence.

3. Test results

The experimental results are presented in normalized form as dimensionless groups (Table 3). This section highlights mainly the evolution of displacement with number of cycles.

The asterisk (*) is applied to other variables too, e.g., F^*_{max}, z^*_{mean}, and denotes the same approach to normalizing as seen in Table 3. The unloading stiffness (K_{un}) is defined in Fig. 10.

In some instances, where relevant, and for the sake of clear visualization, only the mean values of displacement (z_{mean}) and excess pore water pressure ($u_{e,mean}$) are used, as opposed to complete sets of values. These are obtained by computing the average of all samples within a load cycle. z_{mean} may be interpreted as accumulated displacement, and $u_{e,mean}$ as pressure build-up.

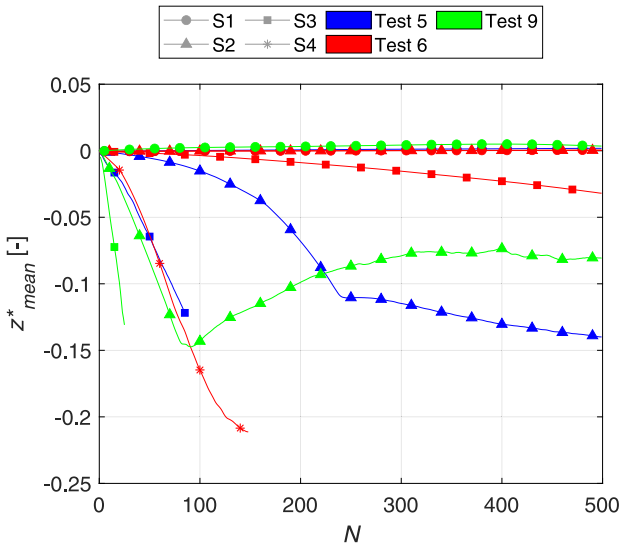

Fig. 14. Output from tests 5, 6, 9. Loading frequency $f = 0.1$ Hz.

The drained tensile capacity (R^d_t) of the model was estimated between 1.8 and 2.1 kN, using the same equipment, by Grecu et al. [29].

3.1. Pre-shearing packets (PS)

In all pre-shearing phases, the loading characteristics and soil properties were nearly identical across tests, leading to similar outcomes (see Fig. 11). After pressurization, the compressive load is reduced gradually from the level attained at the end of installation down to $F_0 = F_{mean} = 5.6$ kN, which constitutes the force magnitude at the beginning of each PS phase. The force reduction process is linear, and takes 10 min, in order to not generate high excess pore pressure.

The model undergoes upward displacement during the first 50 cycles, despite the one-way compressive loading, after which it switches direction, settling steadily. Tests 7 and 9 deviate from the most common trend. There is no measurable change in stiffness and no excess pore pressure build-up in the pre-shearing stage of any test, to potentially serve as explanation for the displacement patterns. Nevertheless, since z^*_{mean} appears relatively small, contained in the interval $(-2 \times 10^{-4}, 5{\times}10^{-4})$, it is assumed that foundation failure did not occur, which indicates successful simulation of normal operating conditions.

3.2. Intermediate packets (I)

Tests 1 and 2 do not contain any intermediate packets, since failure occurred during their first severe loading segments (S1). Fig. 12 displays all I-packets in a tiled layout, grouped by order of appearance.

As expected, net downward displacement takes place in all instances, as a result of one-way compression. The largest share of settlements is within the first 20 to 30 cycles, after which the settlement progression rate decreases considerably. Note that if z^*_{mean} exceeds the threshold of 10^{-3}, then the corresponding test does not reach a subsequent intermediate phase. Surpassing this threshold during packet Ix, therefore, suggests that an ultimate limit state had been almost attained during the preceding packet (Sx) or that it would likely occur during the following packet (Sx+1). As with the PS-packets, unloading stiffness remains constant and mean excess pore pressure is zero throughout I-packets.

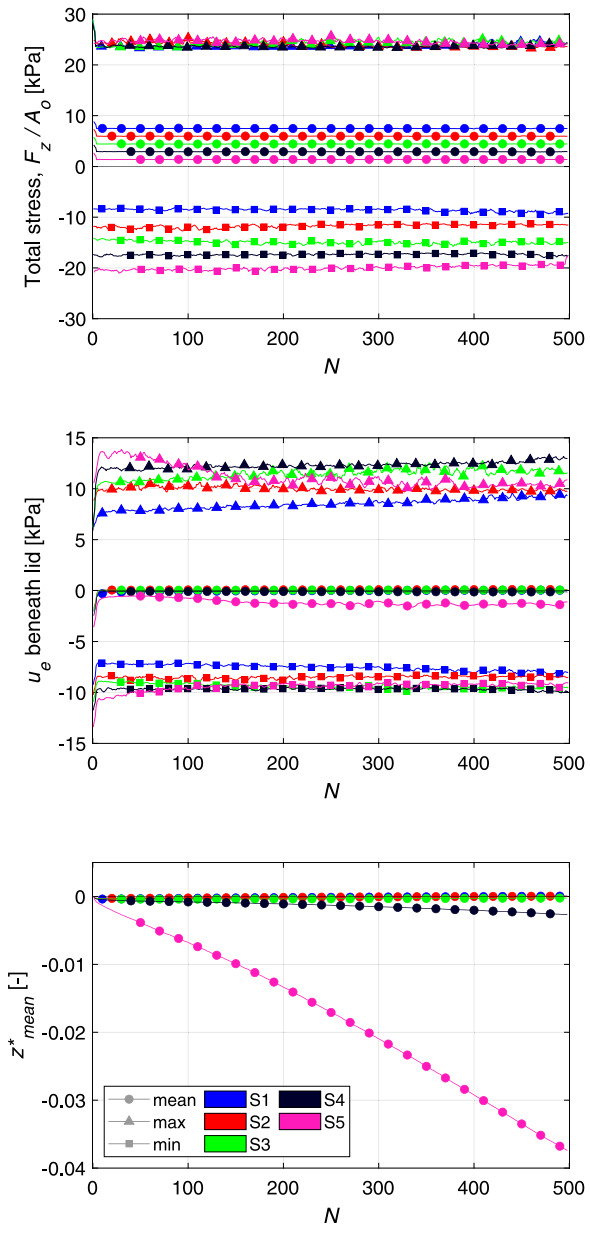

Fig. 15. Output from test 8. Loading frequency $f = 0.5$ Hz.

3.3. Severe load packets (S)

3.3.1. Negative mean force

Tests 1 and 2 represent the only cases where $F_{mean} < 0$. They contain one S-packet each and were both interrupted before completing the programmed loading sequence, due to excessive upward displacement. Fig. 13 shows the results in terms of total stress (F_z/A_o), where $A_o = \pi(D_o/2)^2$; excess pore pressure (u_e) beneath the lid; and normalized mean vertical displacement (z^*_{mean}).

Progressive heave occurs in both tests at relatively high rate, and displacements appear linear to the cycle number. There is no stable part, as failure takes place within the first few load cycles. A notable difference lies in the development of excess pore pressure. In test 1, the patterns of u_e and force are linked directly, while an inverse relationship exists in test 2, where $u_e > 0$, despite the almost pure one-way tensile loading. While examining the aftermaths of these tests, it became clear that a certain soil volume encompassing the bucket had liquefied. On the surface, a circular area with a diameter of approximately $2D_o$ marked the extent of liquefaction. Within this area, the soil could not provide significant resistance, as evidenced by a wrench sinking under its own weight.

3.3.2. Positive mean force

Frequency of 0.1 Hz

In Fig. 14, it is seen that failure precedes the packets that were interrupted due to excessive heave (S3 in tests 5, 9 and S4 in 6). S2 in tests 5 and 9 involve a sudden change of displacement pattern, indicating a change of load transfer mechanism. As with tests where $F_{mean} < 0$, the complete loss of resistance was a result of liquefaction.

Frequency of 0.5 Hz

Test 8 represents the only instance where $f = 0.5$ Hz was applied. Fig. 15 outlines the results of this test.

The gradual decrease of F_{min} (and F_{mean}) with packet number showcases the idea behind the approach to loading. The ranges of u_e are proportional to force ranges. Significant displacements occur in S4 and S5. The $u_{e,max}$ values are visibly highest within the first 100 cycles in S5, while $u_{e,mean}$ are negative throughout the entire loading sequence. Liquefaction had most likely started already during S4, as suggested by the change in rate of displacement accumulation and by the consistently largest $u_{e,max}$ compared to the rest of loading packets.

Frequency of 1 Hz

Out of all conducted experiments, test 7 is the only one where the model did not displace significantly throughout all programmed loading sequences (see Fig. 16). The displacement trends in 3-S5, 4-S3, and 10-S5 resemble 5-S2 and 9-S2 in Fig. 14, where the accumulation rate of displacement becomes zero or reverses after relatively fast development of heave.

Arranging cyclic load packets in series comes with an inherent issue: the effects of soil disturbance due to prior loading. These effects represent an uncontrolled variable that adds uncertainty to conclusions from examinations of packets as individual entities. Thus, it is of interest to gain insight into the magnitude of such effects. To this purpose, packets S1 to S3 in test 4 replicate S3 to S5 in test 3. As Fig. 16 reveals, the displacement patterns are similar between tests, with z^*_{mean} consistently larger by a relatively small margin in test 4 than in 3. Not accounting for the variability of soil density, the prior loading sequences in test 3 (S1 and S2) might have contributed favorably to the stability of the foundation model against cyclic loading of higher amplitudes.

4. Discussion

The main discussion is based on results from severe load packets (S), unless otherwise specified.

4.1. Influence of frequency

To study the effects of loading frequency, three tests were conducted with identical load amplitudes, mean loads, and number of cycles, but with varying f: 0.1 Hz (test 6), 0.5 Hz (test 8), 1 Hz (test 7). Examining Fig. 17, significant discrepancies between the three tests become evident when comparing displacement, excess pore water pressure (EPWP), and stiffness.

A key insight is that vertical displacement and stiffness keep constant levels as long as the mean EPWP stays approximately zero. A noticeable negative spike in $u_{e,mean}$ develops at the beginning of each S-packet, due to the first force cycle starting on the tensile side, that is toward F_{min}. Differences due to variations in loading frequency appear already in S1, where $f = 0.1$ Hz causes overall positive EPWP, while in other tests, negative $u_{e,mean}$ takes approximately 250 cycles to reach nonnegative values. This is linked to the ratio between the rate of dissipation of EPWP and applied loading frequency. At low frequency, there is more time for pressure to dissipate until subsequent unloading. However, an inverse process occurs in the following packets, where $u_{e,mean}$ decreases with cycle number. Two reasons might explain this

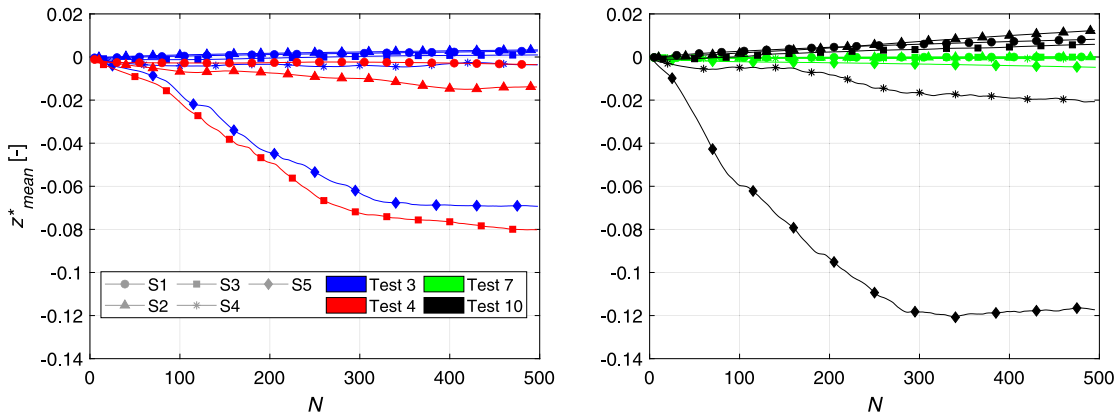

Fig. 16. Output from tests 3, 4, 7, 10. Loading frequency $f = 1$ Hz.

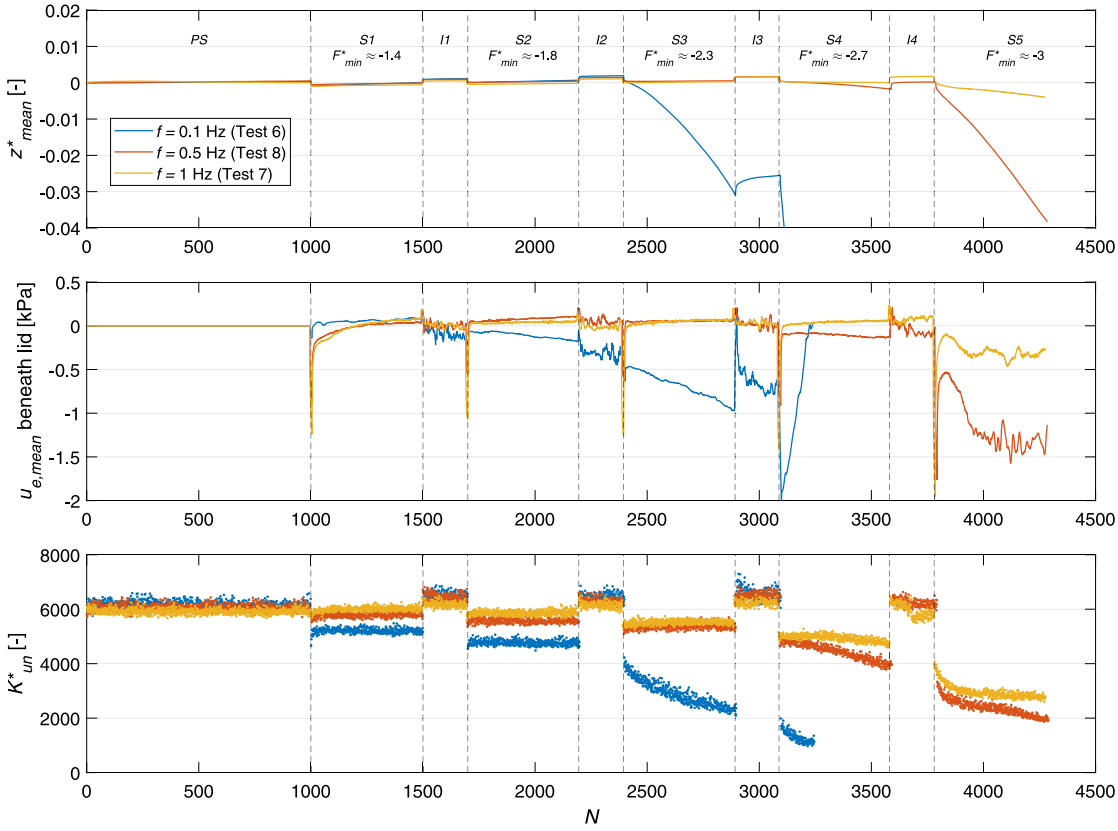

Fig. 17. Mean displacement, excess pore pressure beneath the lid, and unloading stiffness in tests 6, 7, 8. $F^*_{max} \approx 3.7$ across all S-packets.

phenomenon: (a) soil disturbance from the previous loading sequences; (b) effect of interaction between f and force magnitude. Both (a) and (b) stand at the base of how each test progresses through phases.

Given $f = 0.1$ Hz, compared to the pre-shearing stage, the unloading stiffness appears lower by 16 % and 20 % in S1 and S2, respectively. It then rapidly degrades to approximately 30 % in S3, and continues in the same manner in S4, until the upward displacement reaches the pre-established safety limit. Stiffness degradation occurs in all tests, but its rate and onset point depend on the amount of tension and loading frequency. The phenomenon becomes more pronounced and begins earlier with increasing tension and decreasing frequency. Remarkably, during one-way compression (PS- and I-packets), stiffness remains almost unaffected, maintaining constant values regardless of applied frequency and despite prior S-packet loads. This is an important aspect that has implications not only for geotechnical design, but for the entire OWT structure, since foundation stiffness is a determinant of the natural frequency of the system.

Fig. 18 presents normalized force–displacement curves for selected cycles from packets S2 and S3.

For f of 0.5 Hz and 1 Hz, the areas of the hysteresis loops (A^*_{loop}) remain constant, i.e., the same amount of plastic strain energy dissipates during each cycle. States of plastic shakedown persist until $N \approx 150$, followed by ratcheting of a degree that depends inversely on frequency. A similar relationship applies to the range of displacement within one loop ($z^*_{loop} = z^*_{max} - z^*_{min}$), which does not change with the number of cycles, but is affected by frequency: lower f leads to larger z^*_{loop}.

Considering now $f = 0.1$ Hz (test 6), the ratcheting effect spans over the entire loading sequence in S2 and S3, with its magnitude significantly higher in S3. In this packet, the hysteresis loops become gradually larger with the number of cycles, and they distort more on the tensile side than on the compressive one.

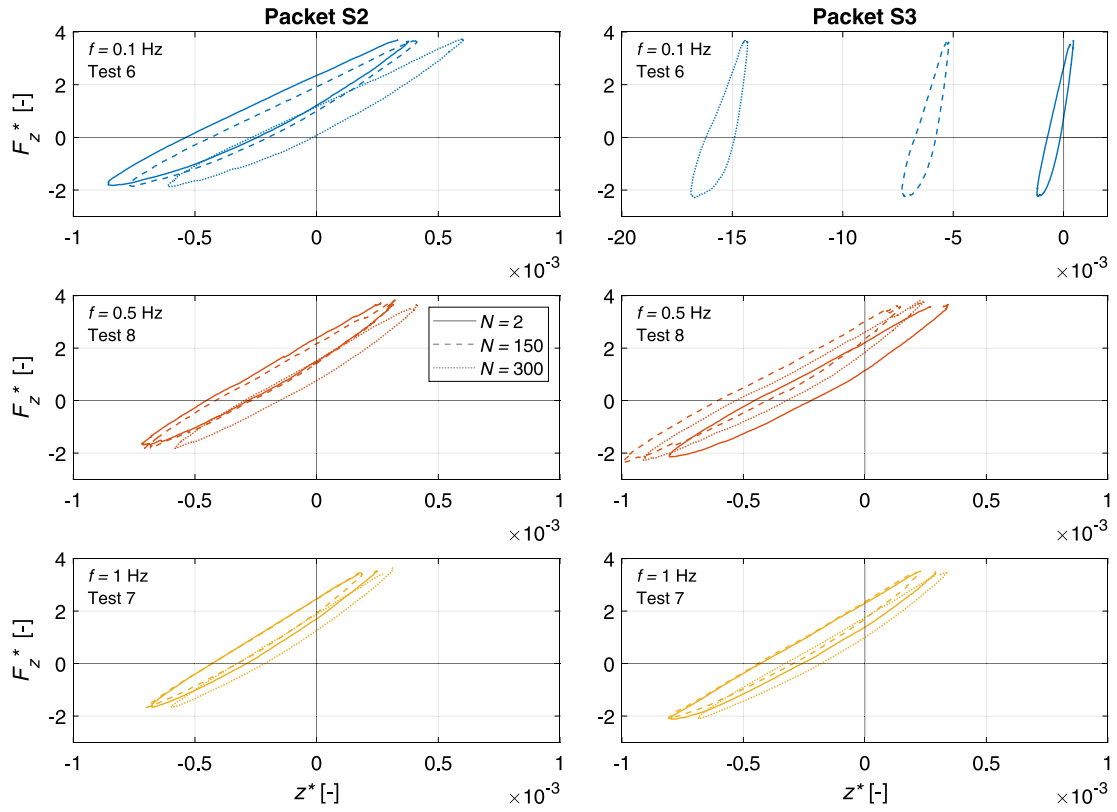

Fig. 18. Hysteresis loops from tests 6, 7, 8; packets S2 and S3.

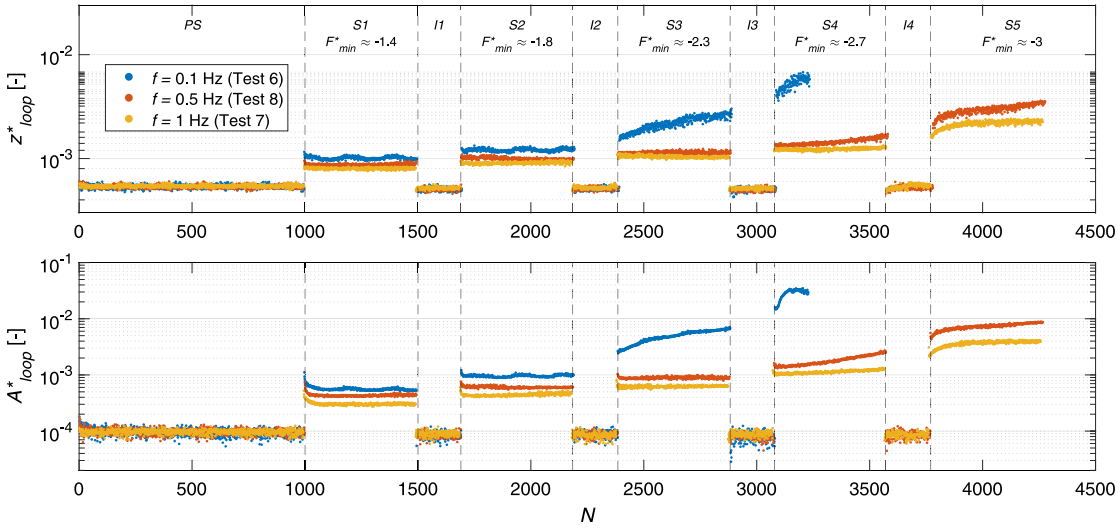

Fig. 19. Displacement ranges and hysteresis loop areas in tests 6, 7, 8. $F^*_{max} \approx 3.7$ across all S-packets.

Another visual representation of the evolution of z^*_{loop} and A^*_{loop} is found in Fig. 19, where these two quantities are plotted against the number of cycles.

Neither z^*_{loop} nor A^*_{loop} change as a result of loading frequency or number of cycles in PS- and I-packets. They only seem marginally affected (I3 and I4) if K^*_{un} had degraded during a prior severe loading sequence (cf. Fig. 17). As to severe loading, it is clear that higher frequency not only causes smaller z^*_{loop} and A^*_{loop}, but also maintains them at a constant and stable value under higher load amplitudes. This is most notable in packet S3, where both the displacement range and the hysteresis loop area increase steadily for $f = 0.1$ Hz, while they remain unchanged for 0.5 Hz and 1 Hz.

4.2. Influence of load magnitude

In tests 3, 7, and 10, the loading frequency was 1 Hz, whereas the mean load and amplitude varied across tests and packets. Fig. 20 summarizes the load characteristics linked to all packets that make up the aforementioned tests.

The target maximum compressive load was set at the same level across packages within a test, however, it is noted that in 3-S5, 10-S4, and 10-S5 it deviates from the rest. The discrepancy between the command and actual force increases for larger target loads in scenarios where a significant EPWP build-up occurs. The evolution of EPWP with

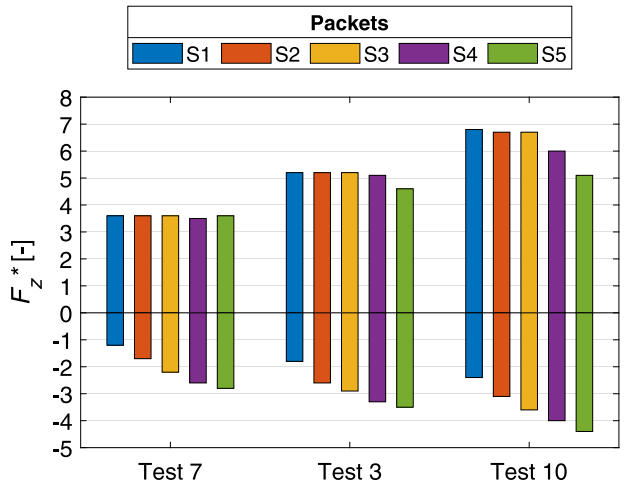

Fig. 20. Cyclic load characteristics in tests 3, 7, 10. Loading frequency $f = 1$ Hz.

the number of cycles, together with that of displacement and stiffness, is displayed in Fig. 21.

The foundation response exhibits high sensitivity to the cyclic load amplitude. In the S-packets of tests 3 and 10, the model settles gradually until S4, where it changes direction and begins heaving. This indicates that the unloading stiffness has degraded sufficiently to allow net upward displacement. The rate of stiffness degradation appears directly proportional to the force amplitude. However, despite equal force increments between tests, the development of K_{un}^* during the last three stages of test 3 is considerably closer to that of test 10 than to test 7. The common trait between 3 and 10 is the relatively large $u_{e,mean}$ in S4, suggesting a likely occurrence of liquefaction, and, consequently, an embedment medium that has near identical properties in the cases of either tests. Notably, the mean EPWP has opposite signs in 3-S4 and 10-S4 (cf. Fig. 13).

Tests 5 and 9, where the S-packets comprised the same load characteristics as applied in tests 3 and 10, but with $f = 0.1$ Hz, showed that such load levels cannot be tolerated given a lower frequency. Referring back to Fig. 14, displacements accumulated rapidly and in similar manners during S2.

4.3. Summary of results

Fig. 22 provides an overview of values of various quantities at the end of each S-packet. The outcomes of the experimental campaign are presented as functions of the controlled variables, i.e., the loading characteristics: frequency and normalized maximum/minimum force.

At frequencies of 0.5 Hz and 1 Hz, displacements accumulate less than at $f = 0.1$ Hz, given similar load magnitudes. As discussed in Section 4.1, higher frequencies contributed to the stability of the model against severe cyclic loads. As F_{mean} approaches 0 and $F_{min}^* < -3$, the values of z_{mean}^* surpass −0.05, meaning significant heave. On the other hand, for $f = 0.1$ Hz, this threshold is exceeded irrespective of F_{mean}. Rapid accumulation of displacement occurred for tests where $F_{mean} < 0$, even though $f = 1$ Hz. The classification of $z_{mean}^* \leq -0.05$ as "significant" is defined by the authors, therefore, its use is restricted to this study only. In general, the context dictates the impact of a certain displacement.

As the upper right plot in Fig. 22 suggests, stiffness decreases if $F_{min}^* < -2.5$ for any maximum force or frequency range. The level of degradation is higher at $f = 0.1$ Hz. There appears to be a correlation between the magnitudes of accumulated displacement, stiffness change and excess pore pressure build-up. It is evident that when the minimum

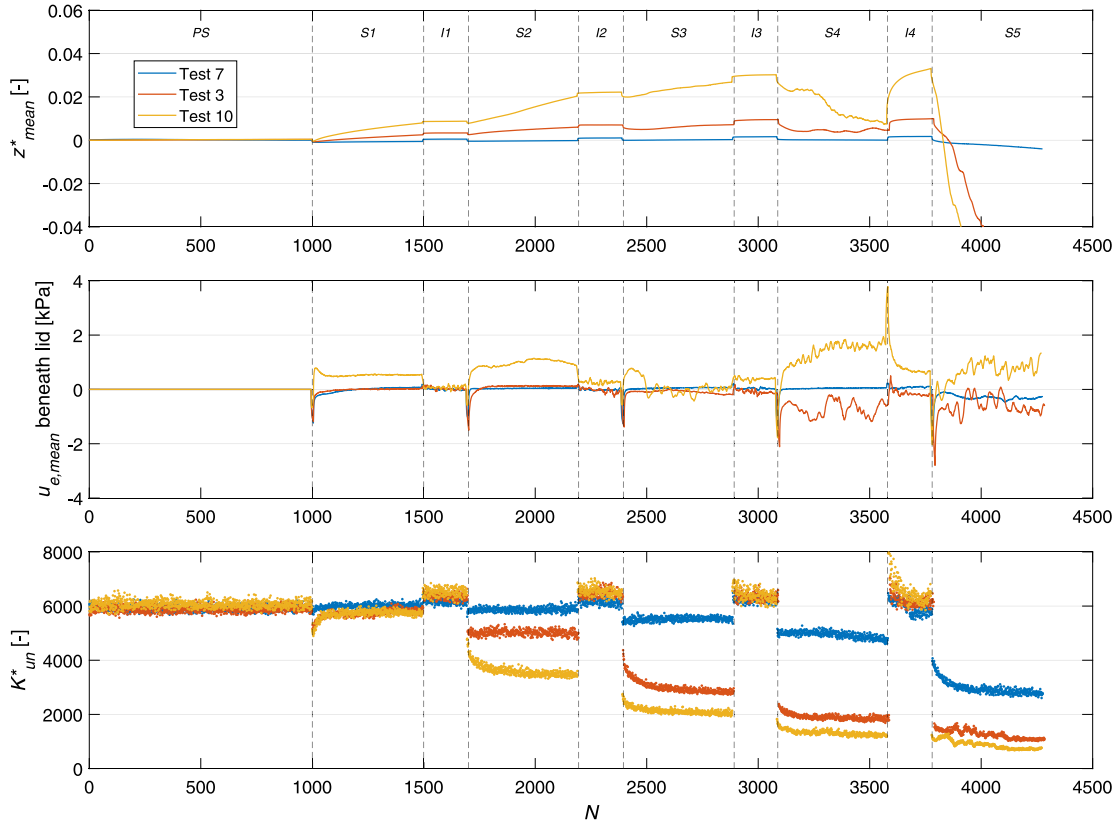

Fig. 21. Mean displacement, excess pore pressure beneath the lid, and unloading stiffness in tests 3, 7, 10. $f = 1$ Hz across all S-packets.

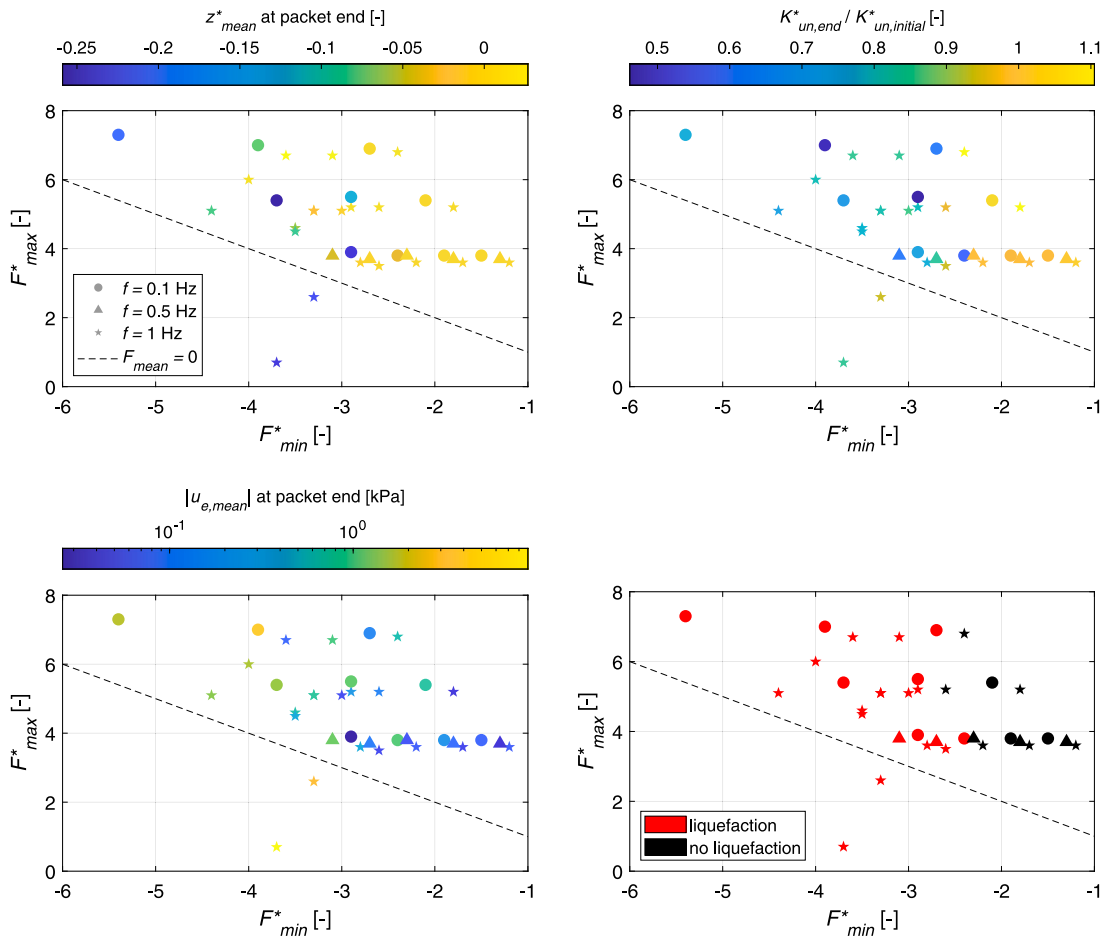

Fig. 22. Final states of physical variables at the end of each S-packet.

force crosses the transitional zone marked by $-3 < F^*_{min} < -2$, severe cyclic loading effects take place. These are due to liquefaction, which can be defined as the state when the ratio of excess pore pressure to effective vertical stress approaches or exceeds 1. For cases where this was condition was met, post-test inspections revealed considerable loosening of the sand mass.

Conducting tests in $1g$ conditions has an intrinsic limitation in the form of relatively low effective stresses. There is a non-linear dependency of dilation angle (ψ) on confining pressure, which was quantified by Ibsen et al. [34] as part of their study on the mechanical properties of Baskarp Sand no. 15. Given the relative density ($D_r \approx 85\%$) and effective vertical stress levels ($\sigma'_v \approx 5\,\text{kPa}$) involved in the present experiments, ψ is evaluated at approximately 11°. The amount of dilation influences the generation of EPWP, which, in turn, affects the occurrence of liquefaction. A result of low effective stresses is the overestimation of the magnitude of the liquefaction phenomenon. In this study, a major part of the soil volume surrounding the foundation was affected, while this might not be the case under in-situ conditions. Therefore, evaluating a full-scale foundation using the presented results would likely lead to a conservative/safe design. The issue of adequate simulation of effective stress state at small scale can be resolved by centrifuge modeling.

Another limiting factor in the current tests is the proximity of impermeable boundaries to the foundation model. Restricting seepage at 1.05 m in the radial direction and 0.9 m in the vertical one from the point of load application might have encouraged the EPWP build-up. A pressure transducer located near the inner edge of the tank showed EPWP fluctuations of magnitudes comparable to the ones recorded on the model surface. Furthermore, this study does not account for the differences in initial soil states resulting from the installation method. Rodriguez et al. [37] compared the effects of jacking against suction-assisted installation, highlighting discrepancies due to redistribution of initial stresses and changes in relative density during installation procedures.

5. Conclusions

The vertical response of suction bucket foundations to cyclic loading was studied by conducting a series of 10 tests on a physical model. The soil medium consisted of dense Baskarp Sand no. 15. The output was examined as a function of loading characteristics: amplitude, mean force, and frequency. As its main focus, this research involved two-way loading, to simulate scenarios of extreme events, while one-way compressive loading represented normal operating conditions. The following items highlight the research outcomes:

- A direct proportionality was observed between loading frequency and foundation stability. Lower frequencies led to more excess pore pressure build-up, which further caused stiffness degradation and permanent displacements. Simultaneously, the areas of hysteresis loops increased with the number of load cycles.
- Force amplitude relates directly to the rate of accumulation of displacement and the magnitude of mean excess pore pressure.
- Given identical mean load and amplitude, failure occurred earlier at a frequency of 0.1 Hz than at 0.5 Hz and 1 Hz. Conversely, while varying all load characteristics except frequency, plastic

deformation appeared correlated with force magnitude. Therefore, a combination of low frequency and large force amplitude represents the most onerous loading scenario.
- Failure occurred immediately upon applying negative mean forces, which confirms the inability of suction buckets to withstand such load types. The severity of unfavorable effects gradually increases as mean load approaches zero.
- Upon applying compressive one-way cyclic loads, stiffness remains constant regardless of cycle number and characteristics of preceding two-way loading sequences, unless large displacements had occurred due to loss of stiffness as a result of liquefaction.
- In terms of liquefaction triggering and its corresponding consequences, a threshold for the magnitude of tensile force was found as $-3 < F^*_{min} < -2$. Applying loads beyond this limit induced liquefaction. The amount of compressive stress within one cycle did not appear to have influence.

These findings may be integrated as part of preliminary assessments of severe cyclic load effects on suction bucket jackets. Particularly, susceptibility to liquefaction can be readily determined using the tensile stress threshold as a criterion.

CRediT authorship contribution statement

Sorin Grecu: Conceptualization, Methodology, Software, Validation, Formal analysis, Investigation, Data curation, Writing – original draft, Writing – review & editing, Visualization. **Amin Barari:** Conceptualization, Methodology, Writing – review & editing, Supervision. **Lars Bo Ibsen:** Conceptualization, Methodology, Resources, Writing – review & editing, Supervision, Project administration, Funding acquisition.

Declaration of competing interest

The authors declare that they have no known competing financial interests or personal relationships that could have appeared to influence the work reported in this paper.

Data availability

The authors do not have permission to share data.

Acknowledgments

This research was funded by the Department of the Built Environment, Aalborg University, under no particular program. The authors gratefully acknowledge the laboratory work of Kristian, Nhivejen, and Redas. The first author extends special thanks to Kim, for countless pleasant talks and technical support of highest quality.

References

[1] Tjelta TI. The suction foundation technology. In: Meyer V, editor. Frontiers in offshore geotechnics III - proceedings of the 3rd international symposium on frontiers in offshore geotechnics (ISFOG 2015), Oslo, Norway. CRC Press; 2015, p. 85–93.
[2] DNVGL. Offshore wind: The power to progress. 2019, URL https://issuu.com/dnvgl/docs/b0faf1968d6d4b65b1c7578b93504fbd.
[3] Bhattacharya S, Biswal S, Aleem M, Amani S, Prabhakaran A, Prakhya G, et al. Seismic design of offshore wind turbines: Good, bad and unknowns. Energies 2021;14(12):3496.
[4] Haddad A, Barari A, Amini R. The remedial performance of suction caisson foundations for offshore wind turbines under seismically induced liquefaction in the seabed: Shake table testing. Mar Struct 2022;83:103171.
[5] Farahani S, Barari A. A simplified procedure for the prediction of liquefaction-induced settlement of offshore wind turbines supported by suction caisson foundation based on effective stress analyses and an ML-based group method of data handling. Earthq Eng Struct Dyn 2023;52(15):5072–98.
[6] Moghaddam A, Barari A, Farahani S, Tabarsa A, Jeng D-S. Effective stress analysis of residual wave-induced liquefaction around caisson-foundations:Bearing capacity degradation and an AI-based framework for predicting settlement. Comput Geotech 2023;159:105364.
[7] Bhattacharya S, Lombardi D, Amani S, Aleem M, Prakhya G, Adhikari S, et al. Physical modelling of offshore wind turbine foundations for TRL (Technology Readiness Level) studies. J Mar Sci Eng 2021;9(6):589.
[8] Barari A, Glitrup K, Christiansen LR, Ibsen LB, Choo YW. Tripod suction caisson foundations for offshore wind energy and their monotonic and cyclic responses in silty sand: Numerical predictions for centrifuge model tests. Soil Dyn Earthq Eng 2021;149:106813.
[9] Grecu S, Ibsen LB, Barari A. Winkler springs for axial response of suction bucket foundations in cohesionless soil. Soils Found 2021;61(1):64–79.
[10] Shonberg A, Harte M, Aghakouchak A, Brown CSD, Pacheco Andrade M, Liingaard MA. Suction bucket jackets for offshore wind turbines: applications from in situ observations. In: Shin Y, editor. Proceedings of TC 209 workshop at the 19th ICSMGE: Foundation design of offshore wind structures, Seoul, South Korea. ISSMGE; 2017, p. 65–77.
[11] Byrne BW, Houlsby GT. Experimental investigations of response of suction caissons to transient vertical loading. J Geotech Geoenviron Eng 2002;128(11):926–39.
[12] Kelly RB, Houlsby GT, Byrne BW. A comparison of field and laboratory tests of caisson foundations in sand and clay. Géotechnique 2006;56(9):617–26.
[13] Kelly RB, Houlsby GT, Byrne BW. Transient vertical loading of model suction caissons in a pressure chamber. Géotechnique 2006;56(10):665–75.
[14] Chen W, Randolph MF. Uplift capacity of suction caissons under sustained and cyclic loading in soft clay. J Geotech Geoenviron Eng 2007;133(11):1352–63.
[15] Hung LC, Lee S, Tran NX, Kim SR. Experimental investigation of the vertical pullout cyclic response of bucket foundations in sand. Appl Ocean Res 2017;68:325–35.
[16] Nielsen SD, Ibsen LB, Nielsen BN. Response of cyclic-loaded bucket foundations in saturated dense sand. J Geotech Geoenviron Eng 2017;143(11):04017086.
[17] Vaitkune E, Ibsen LB, Nielsen BN. Bucket foundation model testing under tensile axial loading. Can Geotech J 2017;54(5):720–8.
[18] Bienen B, Klinkvort RT, O'Loughlin CD, Zhu F, Byrne BW. Suction caissons in dense sand, part II: Vertical cyclic loading into tension. Géotechnique 2018;68(11):953–67.
[19] Gütz P. Tensile loaded suction bucket foundations for offshore structures in sand (Ph.D. thesis), Leibniz University Hannover; 2020.
[20] Jeong YH, Kim JH, Manandhar S, Ha JG, Park HJ, Kim DS. Centrifuge modelling of drained pullout and compression cyclic behaviour of suction bucket. Int J Phys Modell Geotech 2020;20(2):59–70.
[21] Jeong YH, Ko KW, Kim DS, Kim JH. Studies on cyclic behavior of tripod suction bucket foundation system supporting offshore wind turbine using centrifuge model test. Wind Energy 2021;24(5):515–29.
[22] Jeong YH, Lee SW, Kim JH. Centrifuge modeling for the evaluation of the cyclic behavior of offshore wind turbine with tripod foundation. Appl Sci 2021;11(4):1718.
[23] Low HE, Zhu F, Mohr H, Erbrich C, Watson P, Bransby MF, et al. Cyclic loading of offshore wind turbine suction bucket foundations in sand: The importance of loading frequency. In: 4th international symposium on frontiers in offshore geotechnics (ISFOG 2020), Austin, TX, USA. (December):Austin; 2020, p. 321–31.
[24] Stapelfeldt M, Bienen B, Grabe J. The influence of the drainage regime on the installation and the response to vertical cyclic loading of suction caissons in dense sand. Ocean Eng 2020;215:107105.
[25] Stapelfeldt M, Bienen B, Grabe J. Influence of low-permeability layers on the installation and the response to vertical cyclic loading of suction caissons. J Geotech Geoenviron Eng 2021;147(8):04021076.
[26] Zhang Y, Sudhakaran K, Askarinejad A. Centrifuge modelling of suction caissons subjected to cyclic loading in tension. In: Proceedings of the 4th European conference on physical modelling in geotechnics. 2020, p. 263–8.
[27] Zhao L, Bransby MF, Gaudin C. Centrifuge observations on multidirectional loading of a suction caisson in dense sand. Acta Geotech 2020;15(6):1439–51.
[28] Gütz P, Achmus M. Suction bucket foundations under cyclic tensile loading – physical and numerical modeling. Geotech Test J 2021;44(3):20200056.
[29] Grecu S, Ibsen LB, Barari A. Effects of drainage conditions and suction pressure on tensile response of bucket foundations: An experimental study. Ocean Eng 2023;277:114277.
[30] Cathie D, Irvine J, Houlsby G, Byrne B, Buykx S, Dekker M, et al. Suction installed caisson foundations for offshore wind: design guidelines. The Carbon Trust; 2019.
[31] DNVGL. Recommended practice: offshore soil mechanics and geotechnical engineering (DNVGL-RP-C212). DNV-GL; 2019.
[32] Ibsen LB, Bødker L. Baskarp sand No. 15: data report 9301, Aalborg University; 1994.

[33] Borup M, Hedegaard J. Baskarp sand No. 15: data report 9403, Aalborg University; 1995.
[34] Ibsen LB, Hanson M, Hjort T, Thaarup M. MC-parameter calibration of baskarp sand No. 15: DCE technical report No. 62, Aalborg University; 2009.
[35] Barari A, Ibsen LB, Taghavi Ghalesari A, Larsen KA. Embedment effects on vertical bearing capacity of offshore bucket foundations on cohesionless soil. Int J Geomech 2017;17(4):04016110.
[36] Andersen KH. Cyclic soil parameters for offshore foundation design. In: Meyer V, editor. Frontiers in offshore geotechnics III - proceedings of the 3rd international symposium on frontiers in offshore geotechnics (ISFOG 2015), Oslo, Norway. CRC Press; 2015, p. 5–82.
[37] Rodriguez FMG, Ibsen LB, Koteras AK, Barari A. Investigation of the penetration resistance coefficients for the CPT-based method for suction bucket foundation installation in sand. Int J Geomech 2022;22(6):04022063.